Hemispherical digital optical condensers with no lenses, mirrors, or moving parts

Daniel Dominguez,[1,2] Luis Molina,[3] Darshan B. Desai,[1] Trevor O'Loughlin,[1] Ayrton. A. Bernussi,[2,4] and Luis Grave de Peralta[1,2,*]

[1]*Department of Physics, Texas Tech University, Lubbock, Texas 79409, USA*
[2]*Nano Tech Center, Texas Tech University, Lubbock, Texas 79409, USA*
[3]*LJ Technologies, 1041 E 24 St, Hialeah, Florida 331013, USA*
[4]*Department of Electrical and Computer Engineering, Texas Tech University, Lubbock, Texas 79409, USA*
**luis.grave-de-peralta@ttu.edu*

Abstract: We present a simple method for obtaining direct non-scanning images in the far-field with subwavelength resolution. Our approach relies on the use of a digital optical condenser comprised of an array of light emitting diodes uniformly distributed inside of a hollow hemisphere. We demonstrate experimental observation of minimum feature sizes of the order of λ/6 with the proposed technique. Although our experiments were performed at visible frequencies, we anticipate that the proposed approach to subwavelength resolution can be extended to the ultraviolet and infrared spectral regions.

OCIS codes: (110.0180) Microscopy; (220.4298) Nonimaging optics; (110.2990) Image formation theory; (110.2945) Illumination design; (230.3670) Light-emitting diodes.

References and links

1. J. B. Pendry, "Negative refraction makes a perfect lens," Phys. Rev. Lett. **85**(18), 3966–3969 (2000).
2. Z. Liu, H. Lee, Y. Xiong, C. Sun, and X. Zhang, "Far-field optical hyperlens magnifying sub-diffraction-limited objects," Science **315**(5819), 1686 (2007).
3. H. Köheler, "On Abbe's theory of image formation in the microscope," Opt. Acta (Lond.) **28**(12), 1691–1701 (1981).
4. J. W. Goodman, *Introduction to Fourier Optics* (McGraw-Hill, 1968).
5. E. Betzig, M. Isaacson, and A. Lewis, "Collection mode near field scanning optical microscopy," Appl. Phys. Lett. **51**(25), 2088–2090 (1987).
6. T. A. Klar, S. Jakobs, M. Dyba, A. Egner, and S. W. Hell, "Fluorescence microscopy with diffraction resolution barrier broken by stimulated emission," Proc. Natl. Acad. Sci. U.S.A. **97**(15), 8206–8210 (2000).
7. F. M. Huang, T. S. Kao, V. A. Fedotov, Y. Chen, and N. I. Zheludev, "Nanohole array as a lens," Nano Lett. **8**(8), 2469–2472 (2008).
8. D. O. S. Melville, R. J. Blaikie, and C. R. Wolf, "Submicron imaging with a planar silver lens," Appl. Phys. Lett. **84**(22), 4403–4405 (2004).
9. W. Srituravanich, N. Fang, C. Sun, Q. Luo, and X. Zhang, "Plasmonic nanolithography," Nano Lett. **4**(6), 1085–1088 (2004).
10. S. W. Hell and M. Kroug, "Groung-state depletion fluorescence microscopy, a concept for breaking the diffraction resolution limit," Appl. Phys. B **60**(5), 495–497 (1995).
11. X. Zhuang, "Nano-imaging with STORM," Nat. Photonics **3**(7), 365–367 (2009).
12. G. Shtengel, J. A. Galbraith, C. G. Galbraith, J. Lippincott Schwartz, J. M. Gillette, S. Manley, R. Sougrat, C. M. Waterman, P. Kanchanawong, M. W. Davidson, R. D. Fetter, and H. F. Hess, "Interferometric fluorescent super-resolution microscopy resolves 3D cellular structure," Proc. Natl. Acad. Sci. U.S.A. **106**, 3125–3130 (2009).
13. Z. Liu, S. Durant, H. Lee, Y. Pikus, Y. Xiong, C. Sun, and X. Zhang, "Experimental studies of far-field superlens for sub-diffractional optical imaging," Opt. Express **15**(11), 6947–6954 (2007).
14. Z. Liu, S. Durant, H. Lee, Y. Pikus, N. Fang, Y. Xiong, C. Sun, and X. Zhang, "Far-field optical superlens," Nano Lett. **7**(2), 403–408 (2007).
15. H. Lee, Z. Liu, Y. Xiong, C. Sun, and X. Zhang, "Development of optical hyperlens for imaging below the diffraction limit," Opt. Express **15**(24), 15886–15891 (2007).
16. S. P. Frisbie, C. Chesnutt, M. E. Holtz, A. Krishnan, L. Grave de Peralta, and A. A. Bernussi, "Image formation in wide-field microscopes based on leakage of surface plasmon-coupled fluorescence," IEEE Photon. Journal **1**(2), 153–162 (2009).

#201793 - $15.00 USD Received 21 Nov 2013; revised 26 Feb 2014; accepted 10 Mar 2014; published 18 Mar 2014

17. R. Rodriguez, C. J. Regan, A. Ruiz-Columbié, W. Agutu, A. A. Bernussi, and L. Grave de Peralta, "Study of plasmonic crystals using Fourier-plane images obtained with plasmon tomography far-field superlenses," J. Appl. Phys. **110**(8), 083109 (2011).
18. C. J. Regan, R. Rodriguez, S. C. Gourshetty, L. Grave de Peralta, and A. A. Bernussi, "Imaging nanoscale features with plasmon-coupled leakage radiation far-field superlenses," Opt. Express **20**(19), 20827–20834 (2012).
19. L. Grave de Peralta, C. J. Regan, and A. A. Bernussi, "SPP tomography: a simple wide-field nanoscope," Scanning **35**(4), 246–252 (2013).
20. C. J. Regan, D. Dominguez, A. A. Bernussi, and L. Grave de Peralta, "Far-field optical superlens without metal," J. Appl. Phys. **113**(18), 183105 (2013).
21. R. Lopez-Boada, C. J. Regan, D. Dominguez, A. A. Bernussi, and L. Grave de Peralta, "Fundaments of optical far-field subwavelength resolution based on illumination with surface waves," Opt. Express **21**(10), 11928–11942 (2013).
22. A. Vainrub, O. Pustovyy, and V. Vodyanoy, "Resolution of 90 nm (λ/5) in an optical transmission microscope with an annular condenser," Opt. Lett. **31**(19), 2855–2857 (2006).
23. H. H. Hopkins and P. M. Barham, "The influence of the condenser on microscopic resolution," Proc. Phys. Soc. **63**(10), 737–744 (1950).
24. M. Born, and E. Wolf, *Priciples* of *Optics* (Pergamon Press, 1975).
25. LJ Technologies, 1041 E 24 St, Hialeah, Fl 331013, USA.
26. D. O. S. Melville and R. J. Blaikie, "Super-resolution imaging through a planar silver layer," Opt. Express **13**(6), 2127–2134 (2005).
27. W. Srituravanich, N. Fang, C. Sun, Q. Luo, and X. Zhang, "Plasmonic nanolithography," Nano Lett. **4**(6), 1085–1088 (2004).
28. P. Chaturvedi, W. Wu, V. J. Logeeswaran, Z. Yu, M. S. Islam, S. Y. Wang, R. S. Williams, and N. X. Fang, "A smooth optical superlens," Appl. Phys. Lett. **96**(4), 043102 (2010).
29. E. Hetcht, *Optics*, 3rd ed. (Addison Wesley, 1998).
30. Y. Kuznetsova, A. Neumann, and S. R. J. Brueck, "Imaging interferometric microscopy-approaching the linear systems limits of optical resolution," Opt. Express **15**(11), 6651–6663 (2007).
31. S. Durant, Z. Liu, J. M. Steele, and X. Zhang, "Theory of the transmission properties of an optical far-field superlens for imaging beyond the diffraction limit," J. Opt. Soc. Am. B **23**(11), 2383–2392 (2006).
32. G. Zheng, C. Kolner, and C. Yang, "Microscopy refocusing and dark-field imaging by using a simple LED array," Opt. Lett. **36**(20), 3987–3989 (2011).

1. Introduction

Optical microscopy is a well-established technique with a variety of available configurations, illumination sources, and imaging detectors; it is a far-field contactless technique, is simple to use, the samples can be imaged under different environmental conditions, and it is usually cost-effective. These characteristics make optical microscopy an ideal candidate to address the observational needs of sub-cellular biology, as well as the characterization challenges posed by the development of advanced nanofabrication techniques used in the realization of novel materials and devices with nanoscale features. However, it is well-known, from the Abbe's theory of image formation and Fourier optics, that the intrinsic diffraction limit of light prevents conventional optical microscopes from being able to image features with subwavelength dimensions. Optical microscopes using a common illumination source, which produces a collimated beam of light that is incident perpendicular to the sample under observation, are diffraction-limited to spatial periods (p) larger than $\sim\lambda_o/NA$ [1–4], where NA is the numerical aperture of the microscope objective lens, and λ_o is the free-space wavelength of the illumination source. Ground-breaking approaches, however, have been proposed and implemented to overcome this fundamental diffraction limit. Optical images with subwavelength resolution have been achieved with several scanning techniques [5–7] and non-scanning near-field approaches [8,9]. Super-resolution fluorescence microscopy techniques are now commonly used in biological far-field imaging. In deterministic techniques, such as stimulated emission depletion (STED) microscopy [10], fluorophores with a nonlinear excitation response are used. In stochastical single-molecule localization methods, such as stochastical optical reconstruction (STORM) and interferometric photo-activated localization (IPALM) microscopies [11–12], the complex temporal behavior of the fluorophore's response makes them resolvable in time. Wide-field (non-scanning) images with subwavelength resolution have also been obtained in the far-field by numerical

#201793 - $15.00 USD Received 21 Nov 2013; revised 26 Feb 2014; accepted 10 Mar 2014; published 18 Mar 2014

reconstruction of the Moiré patterns formed directly in the image plane of the microscope [13,14], or by using multilayer hyperlenses [15]. However, all of the above-mentioned optical imaging techniques with subwavelength resolution require sophisticated sample preparation, fabrication, or extensive numerical image post-processing.

We have been exploring alternative optical techniques that can provide subwavelength resolution while preserving the simplicity of traditional optical microscopy and where the images are formed directly in the microscope's camera without the need of any numerical reconstruction, sample tagging, or use of samples with complex multilayer structures [16–21]. While investigating the physical principles responsible for the subwavelength resolution capabilities of optical far-field superlenses without metal [20], we realized that the specific nature of the surface waves used for illuminating the object under observation is not a determinant factor for obtaining subwavelength resolution [21]. Moreover, since the discovery of the optical condenser by Abbe in 1873, it is well known that the excitation of surface waves is not a necessary requirement for achieving wide-field images with better resolution than λ_o/NA [3, 22,23]. By illuminating the samples with extreme inclined illumination, optical condensers can reduce the minimum period observable by an optical microscope by half, i.e., $p_{min}\sim\lambda_o/(2NA)$ [3, 22,23]. This expression is also the well-known Rayleigh resolution limit of optical microscopes [23,24]. Typical condensers for optical microscopes are formed by a combination of lenses or mirrors and mechanically deformable diaphragms designed to illuminate the sample with a cone or hollow cone of light. They are then the oldest and simplest known approach to subwavelength resolution. In this work, we present experiments using a digital optical condenser comprised of an array of light emitting diodes (LED) uniformly distributed inside of a hollow hemisphere [25]. We demonstrate that, similar to traditional optical condensers, the digital optical condenser used in this work allows for far-field optical subwavelength resolution in the range $\lambda_o/(2NA) < p_{min} < \lambda_o/NA$ based on imaging by collection of directly transmitted light that is not coupled to evanescent waves. It should be emphasized that the digital condenser's subwavelength resolution range $\lambda_o/(2NA) < p_{min} < \lambda_o/NA$ is comparable to subwavelength resolution values previously reported using different superlens approaches [2, 14, 18–21, 26,27], which then are not ideal superlenses in the original sense of Pendry's proposal of achieving perfect image reconstruction [1]. For instance, in an experimental confirmation of the original Pendry's practical implementation of a near-field superlens by using a planar layer of silver illuminated near its plasma frequency [1], super-resolution imaging was demonstrated by imaging gratings immersed in a medium having a refractive index $n\sim1.5$ with periods down to 145 nm at 365 nm wavelength [26]. This corresponds to p_{min} = 145 nm > $\lambda_o/(2n)$ = 121nm, where we have considered that the maximum angle of light collection at the near-field is $\theta\sim90°$, therefore $NA = n\sin\theta\sim n$. Similarly, a far-field optical hyperlens was demonstrated by imaging a 150-nm-spaced line-pair object with a NA = 1.4 objective lens at 364 nm wavelength illumination [2]. This corresponds to p_{min} = 150 nm > $\lambda_o/(2NA)$ = 130nm. Nevertheless, it should be emphasized that resolution values smaller than the Rayleigh resolution limit, obtained using superlenses, have been reported [28]. In contrast with traditional optical condensers, samples in our experiments are illuminated by the light emitted in all directions by an LED array. Therefore, no lenses, mirrors, or mechanically moving parts are needed to control the NA of the digital condenser. In addition to experimentally demonstrating the subwavelength resolution capabilities of the digital optical condenser, we analyze the deep connection existing between the observed condenser's subwavelength resolution and the theory previously developed for a Fourier optics description of image formation in microscopes using surface wave illumination superlenses [21].

This paper is organized as follows: In Section 2 we describe the experimental set up and the samples used in the experiments. Section 3 is dedicated to the discussion of the experimental results, and the origin of the observed subwavelength resolution. Finally, the conclusions of this work are given in Section 4.

#201793 - $15.00 USD Received 21 Nov 2013; revised 26 Feb 2014; accepted 10 Mar 2014; published 18 Mar 2014

2. Description of the experiments

Figure 1 shows a schematic illustration of the set up used in our experiments. We used a modified Nikon Elipse Ti inverted microscope with a NA_o = 1.49, 100 × oil immersion oil objective lens.

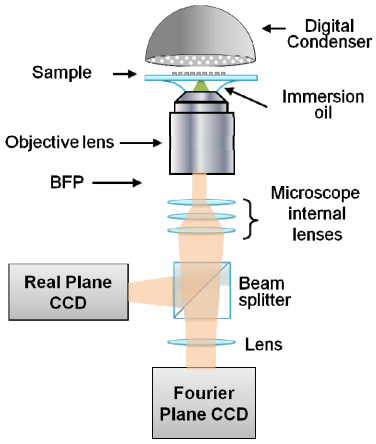

Fig. 1. Schematic illustration of the experimental set up used in our experiments.

Figure 2(a) shows a schematic illustration of the cross-section structure of the sample used in our experiments. We fabricated periodic structures consisting of cylindrical Cr pillars 35 nm tall with varying periodicity p, and diameters $d = p/2$ arranged in a lattice with square symmetry, over a ~150 μm thick glass cover slip. The glass cover slip with the two dimensional (2D) array of Cr pillars, which is the object to be imaged, was then placed for observation in an inverted microscope as it is shown in Fig. 1. In all the experiments described in this work the microscope's built-in illumination source was substituted by a digital optical condenser [25]. This was the sole change introduced into the microscope setup used in our experiments.

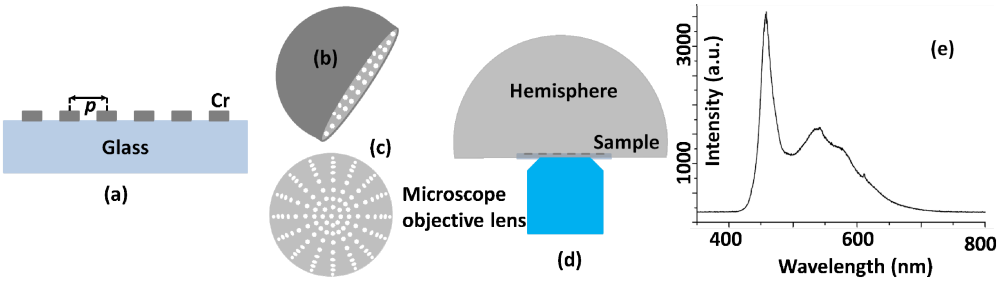

Fig. 2. (a) Cross-section schematic illustration of the samples used in the experiments. Cr discs form a 2D periodic structure with square symmetry and period p over a glass cover slip. Schematic illustration of (b) lateral and (c) bottom views of the digital condenser. White spots represent a 2D LED array distributed uniformly in the internal surface of the hemisphere-shaped light source. (d) Schematic illustration of the relative positions of the hemisphere-shaped condenser, the sample, and the microscope objective lens. (e) LEDs emission spectrum.

Figures 2(b)-2(c) shows schematic illustrations of the hemisphere-shaped digital condenser. The condenser contains a 2D array formed by 560 white-light LEDs distributed uniformly in the internal surface of a rigid hollow hemisphere with a 10 cm radius of curvature. Figure 2(e) shows the LEDs emission spectrum, which has a dominant narrow peak at λ_o~460 nm and a much broader band centered at λ_o~540 nm . Each LED includes a microlens for improving the directionality of the emitted light. All LEDs were electrically

#201793 - $15.00 USD Received 21 Nov 2013; revised 26 Feb 2014; accepted 10 Mar 2014; published 18 Mar 2014

connected, and an external power supply controlled the overall intensity of the LEDs. As it is illustrated in Fig. 2(d), the digital condenser was placed just on top of the glass cover slip. Then, the object under observation was illuminated by LED light emitted in all directions. This is in contrast with the microscope's built-in source of illumination, which produces a collimated beam of light impinging vertically on the top of the sample. As it is illustrated in Fig. 1, real plane (RP) and Fourier plane (FP) images where collected by the two charge coupled device (CCD) cameras of the microscope [16].

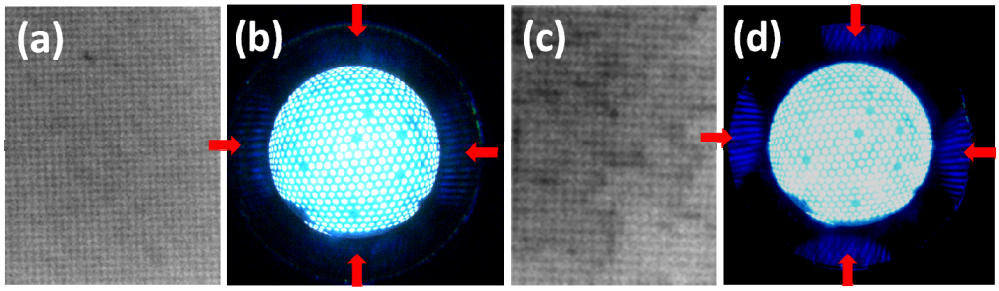

Fig. 3. (a), (c) RP and (b), (d) FP images obtained with the digital condenser-microscope arrangement corresponding to a 2D array of Cr pillars with a period of (a-b) 260 nm and (c-d) 220 nm. Arrows point to the first order diffraction features.

Figure 3 shows RP and FP images obtained with the condenser-microscope arrangement corresponding to two different 2D arrays of Cr pillars. The fabricated samples with square lattice symmetry with periods 260 nm and 220 nm are clearly observed in the RP images shown in Figs. 3(a) and 3(c), respectively. Both arrays were invisible (RP images with uniform background, not shown) when observed using the built-in white-light top illumination source of the microscope. The corresponding FP images are shown in Figs. 3(b) and 3(d), respectively. FP images are maps of the illumination direction [4, 17]; therefore, the FP images show a mirrored picture of the LED array in the digital condenser. By design, each LED points to the center of the hemisphere, providing illumination in all directions from the horizon to the zenith. Consequently, some evidently missing bright spots in the FP images shown in Figs. 3(b) and 3(d) correspond to non-operational LEDs.

3. Discussion of the experimental results

The digital condenser presented in this work produces similar resolution improvements than traditional microscope optical condensers, but the digital condenser differs fundamentally from the traditional ones since it does not comprise of lenses, mirrors, or mechanically adjustable parts. In addition, the presented digital condenser provides an optimum sample illumination due its hemispherical shape which results in large numerical aperture. There are several similarities between traditional optical condensers [22,23] and superlenses based on illumination with surface waves [18–21]. The minimum observable period (p_{min}) in a microscope using a traditional optical condenser is given by the following equation [23]:

$$p_{\min} = \frac{\lambda_o}{NA_o + NA_c} \tag{1}$$

Where NA_o is the numerical aperture of the objective lens and NA_c is the numerical aperture of the condenser. When $NA_o = NA_c$, Eq. (1) gives the Rayleigh resolution limit. Similarly, the value of p_{min} corresponding to the combination of an optical microscope and a superlens based on illumination with surface waves is given by the following equation [18–21]:

$$p_{\min} = \frac{\lambda_o}{n_1 + n_2} \tag{2}$$

#201793 - $15.00 USD Received 21 Nov 2013; revised 26 Feb 2014; accepted 10 Mar 2014; published 18 Mar 2014

For plasmonic superlenses $n_1 = NA_o$, $n_2 = n_{eff}$, where n_{eff} is the effective refractive index experienced by the surface plasmon polaritons (SSP) excited in the superlens [18,19, 21]; while for superlenses based on the excitation of surface waves related with total internal reflection $n_1 = n_{sup}$, $n_2 = n_{sub}$, where n_{sub} and n_{sup} are the refractive indexes of the mediums below (substrate) and above (superstrate) the sample, respectively [20,21]. Traditional optical condensers illuminate the sample with a cone or hollow cone of light. Illuminating the sample with extreme inclined light produces better resolution [22,23]. Similarly, in microscopes with subwavelength resolution based on illumination with surface waves, the light used for imaging is the leakage radiation, which leaks toward the microscope objective lens with a large angle with respect to the normal to the sample surface [18–21]. As a consequence, the corresponding FP images contain bright rings [16–21] resembling what occurs when traditional optical condensers producing circular illumination are used [22]. In addition, light leaking from a superlens in a particular direction is not coherent with light leaking in another direction [21]. Very similar results occur when a digital optical condenser is used as it is illustrated in Figs. 1-2. Indeed, as it is clearly shown in the FP images shown in Figs. 3(b) and 3(d), different LEDs emit in different directions within a cone, whose intersection with the FP results in the formation of a large disk comprised of numerous bright spots. In addition, light emitted by different LEDs is not coherent with each other. Therefore, similarly to traditional condensers, the light used for imaging in our experimental arrangement (Figs. 1-2) is a cone of transmitted light comprised of multiple beams forming a wide range of angles, which is collected by the microscope objective lens. Consequently, one should expect that the resolution of a microscope that uses a digital optical condenser should be given by an equation similar to Eqs. (1) and (2).

For a periodically structured sample illuminated by a coherent monochromatic plane wave propagating perpendicular to the sample surface, the classical Abbe's theory of image formation states that if, and only if, the first order diffraction spots in the FP images can be collected by the microscope objective lens, then a periodic image will be formed in the RP of the microscope [3,4, 29]. However, if the radiation emitted by the source of illumination is not a plane wave impinging perpendicularly to the sample, then the Abbe's theory statement of image formation should be rephrased as follows: *if a fraction of the first order diffraction features can be captured by the microscope objective lens, then the periodic structure of the object will be visible in the image* [21]. When the illumination source produces surface waves in the sample under investigation, the diffraction features observed in the FP images are rings [18–21]. However, in the experiments described in this work, the basic diffraction feature is the set of bright spots observed in the FP images shown in Fig. 3. In Figs. 3(b) and 3(d) the zero order diffraction corresponds to the central disk formed by numerous bright spots. In addition to the zero order diffraction, a fraction of each of the four first order diffraction disks, pointed by the arrows, can also be clearly observed in the bottom, top, right, and left extremes of these figures. As expected, the observed first order diffraction features are distributed in the FP with the same square symmetry as the fabricated array of Cr pillars. Consequently, in accordance to the above generalized statement of the Abbe's theory of image formation, the nanostructures forming the lattices with square symmetry are clearly observed in the RP images shown in Figs. 3(a) and 3(c). Therefore, by analogy with Eqs. (1) and (2), we propose that the minimum observable period using a digital optical condenser is given by the following equation:

$$p_{\min} = \frac{\lambda_o}{NA_o + n} \tag{3}$$

Where n is the refractive index of the medium on top of the sample. Using Eq. (3) with $n = 1$, for λ_o~460 nm and λ_o~540 nm, we estimate p_{min}~185 nm and p_{min}~220 nm, respectively, which are in a good agreement with the period of 220 nm of the observable lattice in the RP image shown in Fig. 3(c). Alternatively, knowing that the radius of the numerical aperture

#201793 - $15.00 USD Received 21 Nov 2013; revised 26 Feb 2014; accepted 10 Mar 2014; published 18 Mar 2014

observed in the FP images shown in the Figs. 3(b) and 3(d) is NA_o = 1.49, we estimated the radius of the circle containing all the bright spots in these FP images as NA_C~1 [16]; therefore, the same estimate for p_{min} can be obtained using Eq. (1) with the value of NA_C directly obtained from the FP images.

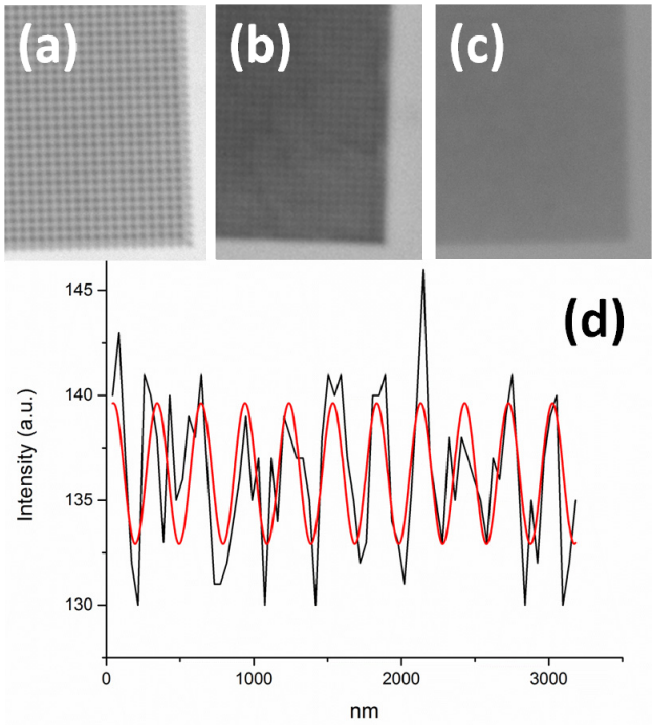

Fig. 4. RP images obtained with the digital condenser-microscope arrangement corresponding to a 2D array of Cr pillars with p = (a) 380 nm, (b) 240 nm and (c) 200 nm. (d) Line profile (black) and fitted sine function (red) corresponding to a periodic sample with p = 300 nm.

The microscope's built-in white-light illumination source emits an almost collimated beam impinging perpendicular to the sample. Therefore, NA_o~0 and in excellent correspondence with Eq. (1), we determined p_{min}~400 nm when we used the microscope with its built-in illumination source. Consequently, the RP images shown in Figs. 3(a), 3(c), 4(a), and 4(b), demonstrate the subwavelength resolution capabilities of the digital condenser-microscope arrangement. Figure 4(d) shows an instance where an intensity line profile (black curve) was obtained from a RP image corresponding to a sample fabricated with p = 300 nm. We fitted the intensity line profile to a sine function represented by the red curve shown in Fig. 4(d). The best fitting was obtained with p~298 nm in excellent correspondence with the period of the fabricated sample. It is worth noting that, as it is evident from the RP image shown in Fig. 4(c), lattices of periods p≤200 nm were not visible in the RP images of the investigated samples. This is in good correspondence with the estimated p_{min}~220 nm for λ_o~540 nm. This suggests that the LED's broad emission band centered at λ_o~540 nm (Fig. 2(e)) limits the resolution of the digital condenser.

#201793 - $15.00 USD Received 21 Nov 2013; revised 26 Feb 2014; accepted 10 Mar 2014; published 18 Mar 2014

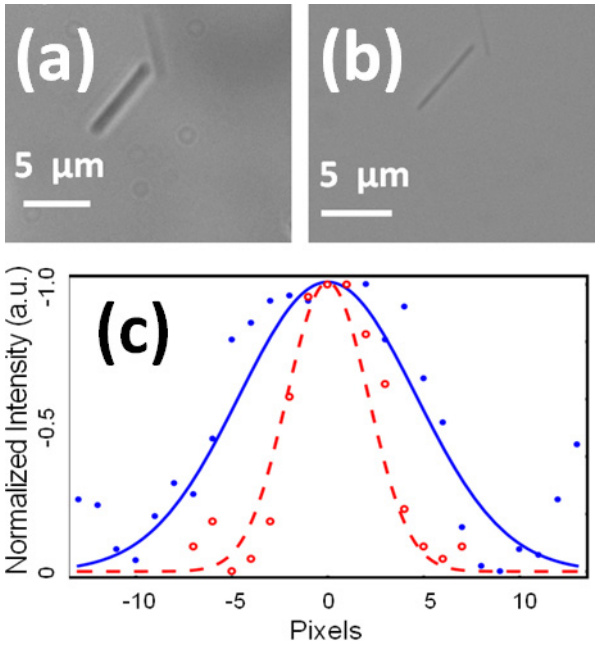

Fig. 5. (a, b) RP of Titanium Dioxide-B wires using (a) microscope's built-in illumination source and (b) the digital condenser. (c) A composition of transversal intensity profiles taken of the same wire using (blue) built-in illumination and (red) digital condenser.

To further explore the resolution enhancement capabilities of the digital condenser we spin-coated Titanium Dioxide-B (TiO_2-B) wires, on a glass coverslip. RP images of the same wires using the microscope's white-light built-in illumination and the digital condenser are shown in Figs. 5(a) and 5(b), respectively. In order to obtain quantitative information about the resolution improvement produced by the digital condenser, we performed a transversal line intensity profile across the center of the same wire for both images (see Fig. 5(c)). The solid and hollow circle symbols in Fig. 5(c) correspond, respectively, to the line profile obtained from Fig. 5(a) and Fig. 5(b). Both data sets were normalized to unity for comparison, inverted about the x-axis (hence the negative intensity values), and fitted to a Gaussian line shape profile. The Gaussian fitting provides a direct qualitative comparison, and allowed us to determine the full-width at half-maximum (FWHM) value of each profile. We determined FWHM = 7 pixels and 12 pixels for the RP images of the same TiO_2-B wire using the microscope built-in illumination and the digital condenser, respectively. This corresponds to a resolving power increase of 1.7 times when the digital condenser was used.

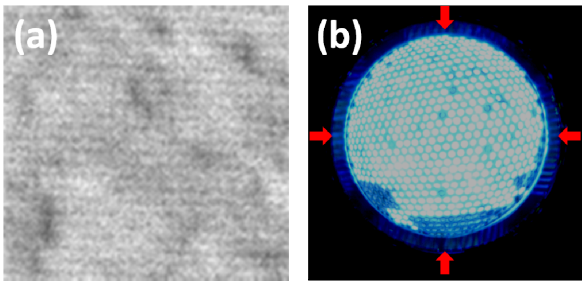

Fig. 6. (a) RP and (b) FP images obtained with the digital condenser-microscope arrangement corresponding to a 2D array of Cr pillars with a period of p = 200 nm covered by a drop of water. Arrows point to the first order diffraction features.

#201793 - $15.00 USD Received 21 Nov 2013; revised 26 Feb 2014; accepted 10 Mar 2014; published 18 Mar 2014

In order to further test the validity of Eq. (3) we imaged a patterned sample with p = 200 nm covered with a drop of water. RP and FP images of this sample are shown in Fig. 6. The RP image (Fig. 6(a)) revealed the presence of the patterned structures. This is also in agreement with the predicted minimum observable period of p_{min}~190 nm when n in Eq. (3) is replaced with the refractive index of water n~1.33 and λ_o~540 nm. The increment in the value of n also produced an increase of the radius of the zero order diffraction disk, as it is clearly seen in the FP image shown in Fig. 6(b). Larger diffraction features result in better resolution, as it is well known from the theory of subwavelength resolution based on illumination with surface waves [18–21]. Sometimes, the figure of merit used to report subwavelength resolution results is the so called lithography critical dimension [30], minimum feature size [27], or half-pitch resolution [14], Δx, given by the by the relation $\Delta x = p_{min}/2$ [31]. Therefore, from Eq. (3), it follows that the Δx value corresponding to the digital condenser-microscope arrangement is given by the following equation:

$$\Delta x = \frac{\lambda_o}{2\left(NA_o + n\right)} \tag{4}$$

Evaluating Eq. (4) for λ_o~540 nm, NA = 1.49, and n~1.33 gives a value of Δx ~λ_o/5.6 = 100 nm. This minimum feature size value can be further decreased by using an array of UV LEDs. A key attribute of the hemispherical digital condenser is excellent uniform illumination with high luminosity. For instance, the hemispherical shape of the digital condenser is particularly well suited for high resolution 2π steradian illumination microscopy.

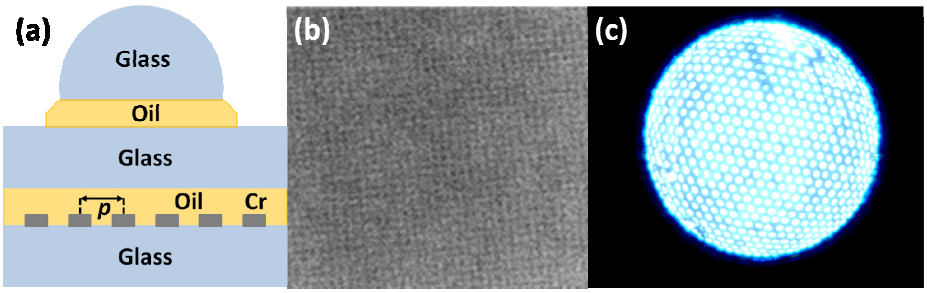

Fig. 7. (a) Schematic illustration of a sample-hemispherical lens arrangement. (b) RP and (c) FP images obtained with a 2π steradian illumination arrangement corresponding to a 2D array of Cr pillars with p = 180 nm.

The minimum resolvable period of a 2D periodic structure in an optical system where the illuminating light is incident from many angles, described by Abbe's theory of image formation, is p_{min}~$\lambda_o/(2n)$; the expression is obtained from Eqs. (1)-(3) when $NA_o = n_1 = NA_c = n_2 = n$. This means that, in the absence of non-linear effects, a periodic structure immersed in a homogeneous medium cannot diffract the incident illumination if the period of the structure is smaller than half of the wavelength of the light in the same medium [30]. This value is half of λ_o/n, which, in turn, is the minimum period capable of diffracting light that is impinging perpendicularly into the sample [29]. Figure 7(a) shows a schematic illustration of a sample designed to obtain the maximum resolution of a linear optical system described by Abbe's theory of image formation. Optical matching oil (n = 1.515) was dropped over a glass coverslip where two-dimensional arrays of Cr pillars were fabricated (as described above), and was then covered by another cover slip. The expected improvement in resolution should come from light that is incident nearly parallel to the sample surface through the periodic structure. However, light incident at these grazing angles on the top coverslip may not illuminate the Cr pillars with the same angle due to the air/glass refraction. To avoid this, we incorporated a hemispherical lens to our sample. Optical matching oil was also dropped over the second coverslip followed by a hemispherical glass lens with 10 mm diameter. The top

#201793 - $15.00 USD Received 21 Nov 2013; revised 26 Feb 2014; accepted 10 Mar 2014; published 18 Mar 2014

coverslip was used to protect the structure, and the optical matching oil was used for index matching between the glass coverslips and lens, thereby creating a homogeneous medium above the Cr structures with refractive index n~1.5. In addition, when the microscope's built-in illumination source was substituted by the digital condenser, illumination from all angles above the plane of sample (a 2π steradian illumination source) was realized. The spherical geometry of both digital condenser and glass lens ensures that the illumination light passes through the 2D Cr pillar array without refraction at the air/glass interface. Consequently, the sample arrangement illustrated in Fig. 7(a) admits illumination with light parallel to the sample surface, which should result in maximum microscope resolution. This was experimentally confirmed by taking RP and FP images of a Cr square lattice array with a period of 180 nm, shown in Figs. 7(b) and 7(c), respectively. Evidently, the zero order diffraction feature corresponding to the digital condenser with the modified sample arrangement, observed in the FP image shown in Fig. 7(c), is larger than the one observed in Fig. 6(b). In fact, the zero order diffraction spot in Fig. 7(c) completely engulfs the *NA* in the FP, indicating that the maximum angle of illumination was achieved and that resolution was increased. As a result, it is difficult to observe the first order diffraction features that would otherwise be expected. However, the sample's periodic structure is clearly visible in the RP image shown in Fig. 7(b).

In the digital optical condenser used in this work, all LEDs are turned ON/OFF simultaneously; therefore, the discrete (digital) character of the illumination could not be fully explored. This could be accomplished by using a digital condenser where each LED could be controlled individually. As it can be seen in the FP images shown in Figs. 3(b), 3(d), 6(b) and 7(c), each LED emits a small cone of light, which produces a bright spot in the FP image. Therefore, direct spatial filtering at the FP could be realized by switching ON/OFF selected groups of LEDs. For instance, turning off the central LEDs of the digital optical condenser could transform the Fourier plane images shown in Figs. 3(b), 3(d), 6(b) and 7(c), by changing the zero order diffraction disk into a ring. This would result in a change from bright-field to dark-field microscopy [32].

4. Conclusions

We presented a simple subwavelength resolution technique based on the use of a digital optical condenser formed by an array of LEDs uniformly distributed over a hollow rigid hemisphere. Using the digital condenser, images with subwavelength resolution are formed directly in the far-field, in the microscope camera, without the need of sample tagging, scanning, or numerical post-processing. We described experiments demonstrating the subwavelength resolution capabilities of a digital condenser-microscope arrangement. We argued that the observed subwavelength resolution can be described by an equation similar to that used to describe the subwavelength resolution of superlenses based on illumination with surface waves and traditional optical condensers. While in our experiments visible light was used, we foresee a direct extension of the presented digital condenser technique to the ultraviolet and infrared spectral regions. A digital infrared condenser, emitting radiation in the 1.2-1.55 μm spectral range, could transform a traditional inverted optical microscope into an infrared microscope enabling the observation of deep subwavelength structures patterned for instance on top of a Si wafer. We anticipate that such digital infrared condenser-microscope arrangement will find multiple applications in the Si-CMOS industries.

Acknowledgments

This work was partially supported by the NSF CAREER Award (ECCS-0954490).

#201793 - $15.00 USD Received 21 Nov 2013; revised 26 Feb 2014; accepted 10 Mar 2014; published 18 Mar 2014